

Wave attenuation in partially saturated porous rocks — New observations and interpretations across scales

EVA CASPARI, QIAOMU QI, SOFIA LOPES, and MAXIM LEBEDEV, Curtin University

BORIS GUREVICH, Curtin University and CSIRO

J. GERMÁN RUBINO, University of Lausanne

DANILO R. VELIS, CONICET, Universidad Nacional de La Plata

MICHAEL B. CLENNELL and TOBIAS M. MÜLLER, CSIRO

Abstract

Seismic waves propagating in porous rocks saturated with two immiscible fluids can be strongly attenuated. Predicting saturation effects on seismic responses requires a sound understanding of attenuation and velocity dependencies on the fluid distribution. Decoding these effects involves interpreting laboratory experiments, analyzing well-log data, and performing numerical simulations. Despite striking differences among scales, flow regimes, and frequency bands, some aspects of wave attenuation can be explained with a single mechanism — wave-induced pressure diffusion. Different facets of wave-induced pressure diffusion can be revealed across scales.

Introduction

A rock whose pore space is occupied by immiscible fluids is referred to as a partially saturated rock. Partial saturation arises when one fluid migrates (or is injected) into a rock, partially replacing the in situ fluid. Because the in situ fluid will not be swept out completely, patches of the fluid phases will be formed. The patches not only exist within one pore but can also extend over many pores, as evidenced by direct laboratory observations (Lebedev et al., 2009; Lei and Xue, 2009; Alemu et al., 2013).

Acoustic monitoring of core-flooding experiments reveals complex wave velocity-saturation (VSR) and attenuation-saturation (ASR) relationships. At the field scale, patchy-saturation scenarios typically are linked to fluid injection into or production from hydrocarbon reservoirs and are thought to affect time-lapse seismic signals (Ajo-Franklin et al., 2013; Villaudy et al., 2013; Vasco et al., 2014). Strongest changes are observed near the injection well. This indicates that patchy saturation can affect sonic responses (Xue et al., 2006). Strong amplitude distortions in the presence of gas chimneys (Yu et al., 2012) possibly are caused by patchy saturation.

Therefore, predicting saturation effects on seismic responses requires a firm understanding of the underlying velocity and attenuation dependencies on pore-fluid distribution. Core-flooding laboratory experiments and reservoir-scale injection/production operations differ by orders of magnitude in length scale. The former typically are monitored by ultrasonic waves and the latter by seismic waves. Furthermore, the flow regimes leading to patchy saturation might differ significantly in both cases with respect to flow rates and driving forces. This makes the modeling and interpretation of VSR and ASR across scales and in different frequency bands a challenging task.

Despite these striking differences, some aspects of wave attenuation can be explained in terms of a single mechanism, wave-induced pressure diffusion (Müller et al., 2010). In this article, we interpret laboratory experiments, analyze well-log data, and perform numerical simulations to reveal different facets of wave-induced pressure diffusion at different scales and frequencies.

Methodological background

If a patchy-saturated rock is probed by seismic waves, fluid-pressure gradients develop across adjacent fluid patches. The induced pressure gradients scale with the fluid-compressibility contrast. These induced pressure gradients vanish (relax) through fluid-pressure diffusion, a process accompanied by friction and thus dissipation. Depending on the relation between patch size and length scale over which pressure diffusion takes place, different regimes occur.

Moreover, we can distinguish three frequency regimes because this diffusion wavelength, similarly to a viscous skin depth, scales with the square root of frequency. In the low-frequency limit, pressure gradients vanish because there has been enough time in one wave cycle for all pressure gradients to equilibrate. If the frequency is high enough, there will be no communication among different fluid pockets, and the induced pressure gradients persist. This causes an overall stiffening of the rock. At intermediate frequencies, wave-induced pressure diffusion leads to dissipation and thus to attenuation and dispersion. This is known as wave-induced fluid flow (WIFF). Note, however, that WIFF does not imply any net fluid flow through the rock.

The three frequency regimes are characterized by distinct velocity-saturation relations. If the porous rock frame itself is homogeneous and saturation is spatially variable, exact bounds exist for the effective elastic properties of the fluid-saturated rock. They are called *uniform* and *patchy* saturation bounds (Mavko and Mukerji, 1998). Because these two bounds correspond to the low- and high-frequency limits, they also are referred to as Gassmann-Wood (GW) and Gassmann-Hill (GH) bounds, respectively. For rock behavior consistent with the Biot-Gassmann theory, the VSR inevitably lies within those bounds for any finite frequency. Only in the limiting cases are the effective elastic properties frequency independent.

Here we focus our study on the attenuation and velocity dispersion caused by wave-induced pressure diffusion on mesoscopic saturation patches. *Mesoscopic* refers to a length scale that is large compared with a typical pore size but small

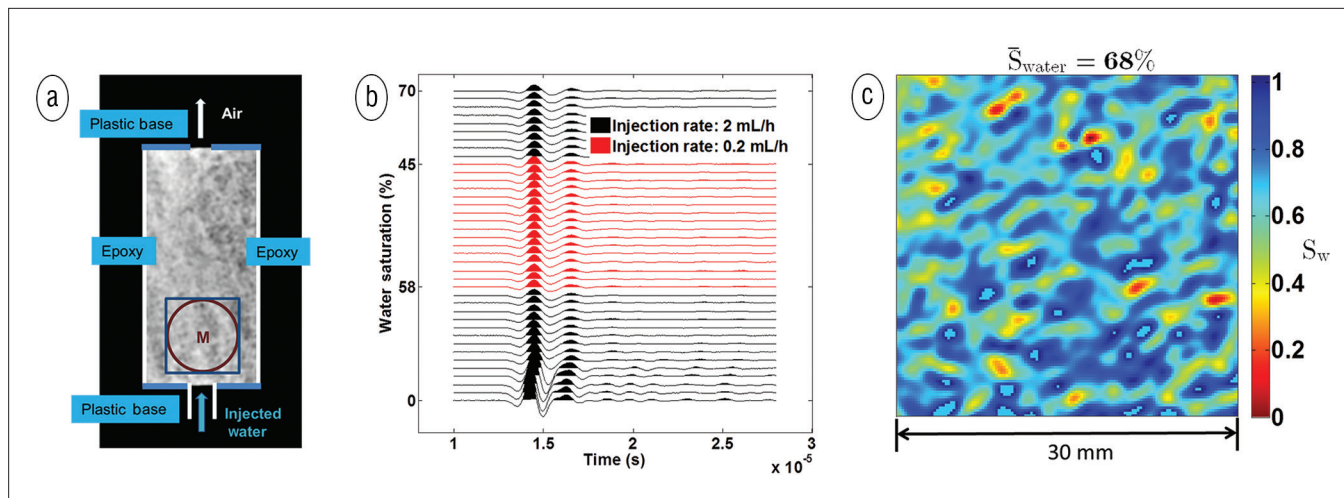


Figure 1. (a) Setup of the dynamic imbibition experiment on Savonnières limestone (porosity 26.5% and permeability 91.5 mD). A CT scan in the axial direction of the sample is embedded in the sketch. Gray color scale represents CT values, a proxy for X-ray absorption. Position of the ultrasonic transducers is marked by M. (b) Ultrasonic waveforms recorded at various levels of water saturation. Black waveforms are recorded when the injection rate is 2 mL/h. Red waveforms correspond to times when the injection rate is 0.2 mL/h. Note the primary-wave amplitude decay while saturation increases as much as 58% and amplitude gain while saturation decreases after switching the injection rate. (c) Water-saturation map (average $S_w = 68\%$) derived from the CT images. Millimeter-scale fluid patches appear. After Lopes et al., 2014, Figure 3.

compared with the wavelength of the propagating wave (Caspari et al., 2011). The focus on mesoscopic length scale has the advantage that models for WIFF can be based on the well-known wave-propagation theory in porous materials developed by Biot (1962).

The dependence of velocity and attenuation on saturation, frequency, and geometric distribution of fluids, particularly the characteristic length scale of fluid patches, can be quantified by the continuous random-media models (CRM) of Müller and Gurevich (2004) and of Toms et al. (2007). Application of those CRM models requires knowledge of the statistical properties of fluid-patch distributions. In mesoscopic models, any pressure-equilibration processes linked to pore-scale heterogeneities are then left out, and their description would require an extension of the theoretical framework, as discussed below.

Laboratory experiments

Perhaps the most detailed insights into the distribution of fluid patches and accompanying evolutions of ultrasonic P-wave velocity and attenuation with saturation can be gained from a recent series of laboratory experiments (Lei and Xue, 2009; Lopes and Lebedev, 2012; Alemu et al., 2013; Lopes et al., 2014). Here we focus on the experimental setup discussed by Lopes et al. (2014). Forced water imbibition into a core sample is monitored by ultrasonic measurements and X-ray computer tomography, which yields information on spatial and temporal fluid distribution. Figure 1a shows the

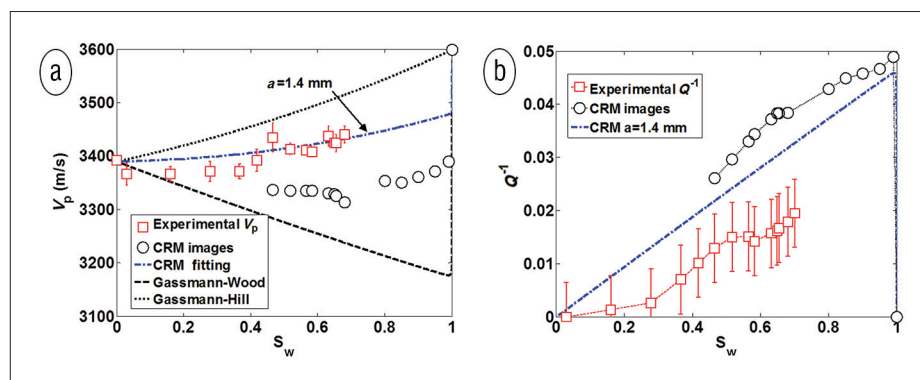


Figure 2. (a) Velocity- and (b) attenuation-saturation relations. Red squares denote experimentally determined velocities from first-break picking and reciprocal quality factor Q^{-1} obtained by the spectral-ratio method. Black circles represent CRM predictions based on statistical attributes derived from the CT images. Dashed-dotted blue lines show best-fit predictions using the CRM model with a constant correlation length, $a = 1.4$ mm.

schematic setup. The imbibition experiment involves a 22-hour nonstop injection of distilled water subdivided into three phases (at a rate of 2 mL/h for ~ 4 h, 0.2 mL/h for ~ 15 h, and 2 mL/h for ~ 3 h).

Using ultrasonic transducers (central frequency 1 MHz), P-waves propagating perpendicular to the core axis are recorded. The resulting waveforms reveal a reduction in amplitude with increasing water saturation and show sensitivity to changes in injection rate (Figure 1b). Saturation maps generated from the CT images allow us to infer the statistical information about fluid distribution, such as the characteristic size of fluid patches (Figure 1c). These saturation images suggest that fluid patches are formed at millimeter scale. These patches extend over several pore spaces and grains but are smaller than the dominant ultrasonic wavelength and thus are interpreted as mesoscopic-scale fluid patches.

From the recorded waveforms, we infer velocities and attenuation as a function of saturation (Figure 2). A comparison of the observed VSR with the uniform and patchy saturation bounds shows that the data points fall between those bounds. A possible reason for deviation from the bounds is wave-induced pressure diffusion. Thus we attempt to model this VSR with the CRM model. It is possible to fit the observed VSR trend using the CRM model with a single Debye correlation function and a correlation length of $a = 1.4$ mm. However, the attenuation predicted by CRM is then twice as large as measured (Figure 2b).

Furthermore, the correlation function extracted from the saturation maps yields velocity and attenuation estimates, shown by black circles in Figure 2. It appears that there is a discrepancy that cannot be explained satisfactorily by the CRM model. A possible explanation related to capillary effects is discussed in the section below on challenges and ambiguities.

Time-lapse log-data modeling

In the well-log environment, fluid patches can affect sonic waveforms. Time-lapse sonic and neutron logs from the Nagaoka CO₂ sequestration experiment (Konishi et al., 2009) provide an opportunity to study the VSR at in situ conditions in the sonic-log frequency band and estimate the corresponding attenuation (Xue et al., 2006; Konishi et al., 2009, Caspari et al., 2011). Konishi et al. (2009) show that the VSR follows a linear trend broadly consistent with the GH bound. Caspari et al. (2011) obtain P-wave velocity-saturation relations at reservoir depth for two thin reservoir sections. Assuming a random distribution of CO₂ patches, Caspari et al. (2011) show that WIFF can be evoked to explain these velocity-saturation relations. Here, we complement these results with the corresponding attenuation estimates.

At the Nagaoka CO₂ test site, 10,400 tonnes of supercritical CO₂ was injected into an onshore saline aquifer at a depth of about 1100 m. The target zone was a porous sandstone interval 12 m thick. Time-lapse data of observation well OB2 40 m downdip from the injection well comprised 13 baseline, 23 monitoring (during injection), and 14 postinjection sonic and neutron-porosity logs. The averages of the first 13 sonic and neutron-porosity logs recorded before the CO₂ breakthrough were used as baseline data

and logs 17 through 26 as monitoring data (Caspari et al., 2011). CO₂ saturation was estimated from differences in the time-lapse neutron logs (Konishi et al., 2009).

Log responses vary with depth in the reservoir zone, indicating that the zone is heterogeneous. Therefore, a VSR inferred from log responses of the whole reservoir zone might be influenced by variations of rock properties with depth and will mask the true VSR. To eliminate the ambiguity caused by this effect, we analyze two 0.5-m-thick intervals with relatively small depth variations. Furthermore, to minimize the problem of random fluctuations in the monitoring logs, time-lapse data points are smoothed in time for each individual depth (Caspari et al., 2011). Figure 3 shows a comparison of these data sets to known VSRs. It can be observed that the data points fall between the bounds of uniform (GW) and patchy (GH) saturation (Caspari et al., 2011).

Fitting a CRM model to each data point allows us to infer characteristic patch sizes of CO₂ (Figure 4a). From this forward modeling, the patch size is estimated at 1 to 5 mm for the shallow interval, but mostly 1 mm for the deeper interval. This demonstrates that patch sizes might be different at different reservoir depths. Because the estimated patch sizes are on

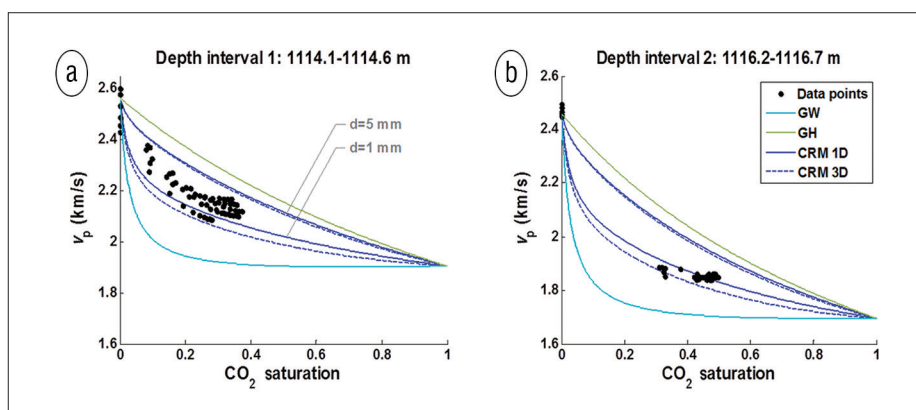


Figure 3. Comparison between VSR models and time-lapse log data for the (a) shallower and (b) deeper depth interval at sonic frequencies. The CRM models correspond to patch sizes (“d”) of 1 and 5 mm. GW, GH, and CRM are Gassmann-Wood, Gassmann-Hill, and continuous random-media models, respectively. After Caspari et al., 2011, Figure 2.

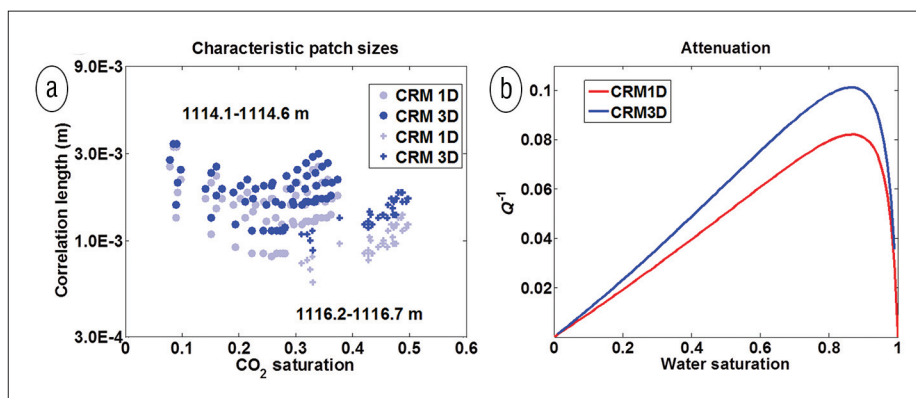


Figure 4. (a) Estimated correlation length (patch sizes) from log data. Circles denote the shallow depth interval and crosses the deeper one. (b) Attenuation versus water saturation for a patch size of 1 mm.

the order of a few millimeters, they are larger than pore-scale features observed in thin sections (Xue et al., 2006). This indicates that wave-induced fluid-pressure diffusion among mesoscopic inhomogeneities can occur at sonic frequencies and can be responsible for attenuation (Caspari et al., 2011).

Figure 4b shows attenuation as a function of water saturation for a patch size of 1 mm. It can be observed that maximum attenuation occurs at low gas saturations (similar to the experimental data mentioned in the previous section). The patch sizes estimated from sonic-log data are on the same order as those observed in the laboratory ultrasound measurements of Lei and Xue (2009) on CO_2 -saturated sandstone. This indicates that similar patch sizes can play a role in ultrasonic and sonic-log measurements. It points to an intriguing possibility that laboratory fluid-injection experiments might be used to simulate in situ conditions in the sonic frequency band (Caspari et al., 2011).

The sonic frequency-band VSR results are limited by the penetration depth of the log measurements and do not permit any conclusion on fluid distribution on a larger scale, such as meter and beyond (Caspari et al., 2011). To understand the effect of fluid patches on attenuation and dispersion at seismic frequencies, we perform seismic simulations.

Simulations of the seismic response at reservoir scale

From the above observations, one expects strong attenuation and dispersion in brine-saturated formations containing supercritical CO_2 patches because of high compressibility contrast among these fluids (Rubino et al., 2011). To understand the implications on seismic signatures, we construct a modeling scenario inspired by the CO_2 storage project at the Sleipner field, Norway, where millions of tonnes of CO_2 have been injected into a major saline aquifer (Utsira Sand Formation).

For the simulations, we employ a poroelastic model of a homogeneous, poorly consolidated sandstone resembling the Utsira Sand. We consider spatially variable CO_2 -brine distributions wherein fluids form randomly shaped patches. These binary fluid distributions are obtained by thresholding realizations of stochastic fractals characterized by a correlation length of 10 cm.

The poroelastic model is subjected to numerical upscaling based on oscillatory compressibility tests (Rubino et al., 2009), which helps to quantify seismic-attenuation

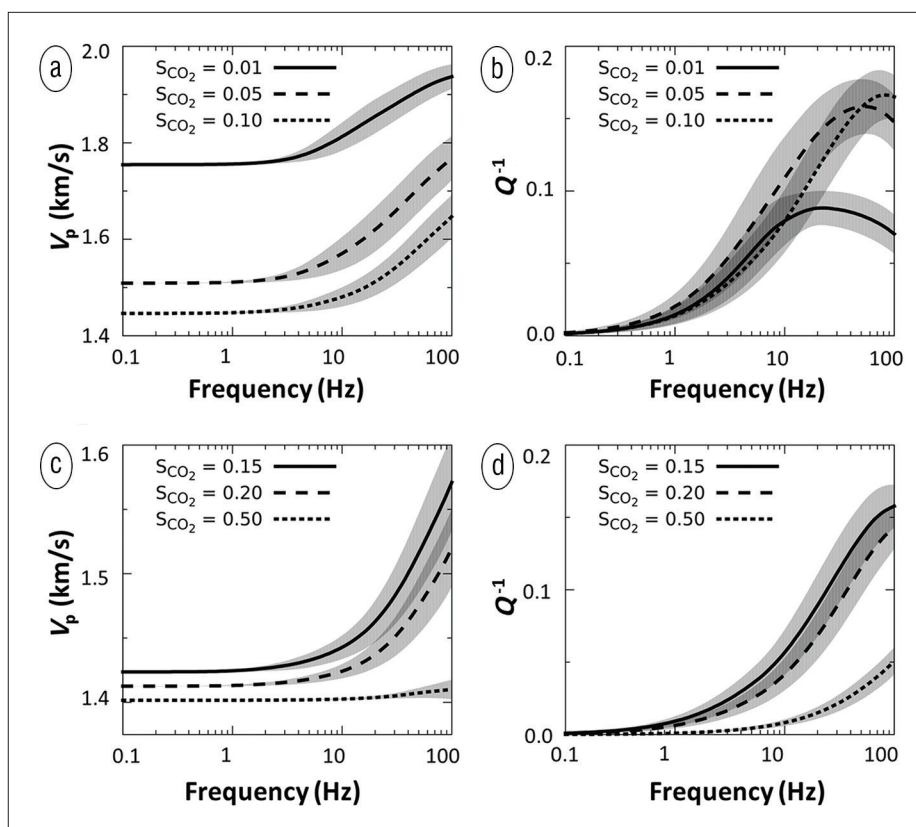


Figure 5. Mean equivalent phase velocity (a and c) and inverse quality factor (b and d) as functions of frequency for different CO_2 saturation levels. Shaded gray areas indicate their corresponding standard deviation intervals. After Rubino et al., 2011, Figures 2, 3, and 5. Used by permission.

and dispersion effects caused by WIFF. By applying this up-scaling in a Monte Carlo manner, the statistical variability of attenuation and dispersion is determined within the seismic frequency band (Figure 5). Strong attenuation, with Q values even below 10, occurs in the seismic frequency band, mainly for CO_2 saturations below 0.5. In addition, significant dispersion effects are observed, with velocity variations of about 10% in the frequency range of 10 to 100 Hz.

Because a poroelastic simulation at the reservoir scale is computationally demanding, especially in the presence of centimeter-scale fluid patches, we determine dynamic-equivalent viscoelastic solids for the mean attenuation and phase velocity at each CO_2 saturation level. These viscoelastic solids are then used to populate differently saturated regions of the geologic model. Solving the viscoelastic wave equation yields synthetic seismograms.

Figure 6a shows the conceptual geologic model used to represent a realistic CO_2 distribution. The CO_2 plume is in a 250-m-thick Utsira-like sandstone embedded between two shale layers (top and bottom gray areas). Within the reservoir, the plume is partitioned into areas with high (about 0.9) and low (below 0.1) CO_2 saturations. The high-saturation zone (horizontal black thin regions) consists of seven layers with thicknesses of 8 to 10 m in their axial parts. The low-saturation (diffuse) zone has CO_2 concentrations decreasing from 0.1 in the axial parts to zero in the outer parts (gray shaded areas).

Figure 6b shows the corresponding zero-offset seismic sections (synthetics). For comparison, we include in Figure 6c the response obtained by replacing the viscoelastic solids with equivalent elastic solids. The latter have the same bulk density and shear velocity, but the P-wave velocity is given

by Gassmann's formula. Examining Figures 6b and 6c, we see strong amplitude distortions, mainly in the axial part of the plume, where most of the diffuse CO₂ accumulations are located. We also can observe kinematic changes. For example, the velocity pushdown produced by the presence of CO₂ is

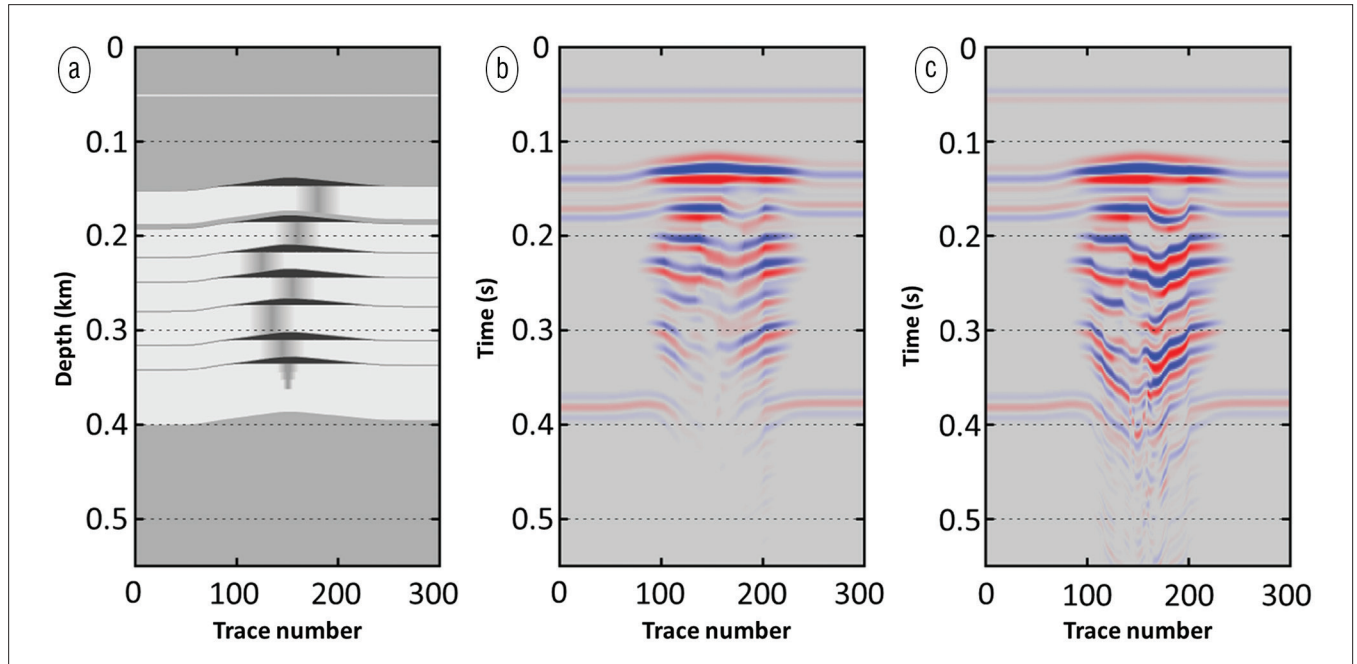


Figure 6. (a) Scheme of the geologic model for Sleipner field (depth relative to a reference level). Black thin areas indicate the main CO₂ component. Narrow gray-shaded areas indicate the presence of a diffuse CO₂ component. (b) Seismic response considering the mesoscopic effects caused by patchy saturation. (c) Seismic response for an equivalent elastic model with P-wave velocity given by Gassmann's formula. After Rubino et al., 2011, Figures 11, 13, and 14. Used by permission.

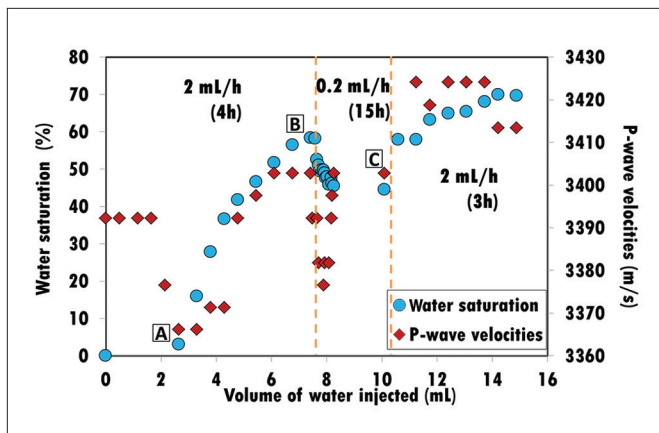


Figure 7. Water imbibition into dry limestone. P-wave velocity (V_p) and water saturation (S_w) evolution with volume of injected water. Three distinctive points can be observed. A: Once water enters the ultrasonically monitored position (Figure 1), V_p and S_w increase. B: After injection rate is decreased, V_p and S_w decrease first sharply and then gradually. C: V_p and S_w increase again once the injection rate is switched back to its initial value. After Lopes et al., 2014, Figure 10. Used by permission.

more significant when dispersion is neglected, as shown in Figure 6c.

These results suggest that WIFF in the presence of centimeter-scale fluid patches might produce noticeable changes in seismic data. Consequently, the nature of fluid distributions and the proper modeling of the seismic response constitute key aspects when characterizing reservoirs with two immiscible fluids of differing compressibility.

Challenges and ambiguities

Fluid-patch formation and evolution are dictated by two-phase flow through porous rocks. This means the acoustically monitored imbibition experiments possibly can give us some insight into the relation between wave attenuation and two-phase flow concepts. As observed in Figure 1, injection-rate changes during imbibition have a direct expression in ultrasonic waveforms. The corresponding P-wave velocity as a function of saturation and injection rate is summarized in Figure 7.

It can be seen that the P-wave velocity and saturation respond in a relaxation-type manner to injection rate changes. This response can be explained by a redistribution of the forces driving the flow (Lopes et al., 2014). Then, for example, the question arises whether capillary forces will produce a net effect on the macroscale so that WIFF signatures are affected. Here, we can make use of the conceptual model of Tserkovnyak and Johnson (2003), which assumes that capillary action is responsible for an interfacial tension between the two fluid phases. The latter causes an overall stiffening and hence an elevated Gassmann-Wood lower bound.

On incorporating this capillarity effect into the CRM model, we obtain modified estimates for attenuation and dispersion (Figure 8). Interestingly, this capillarity-extended CRM model is capable of modeling the VSR and ASR shown

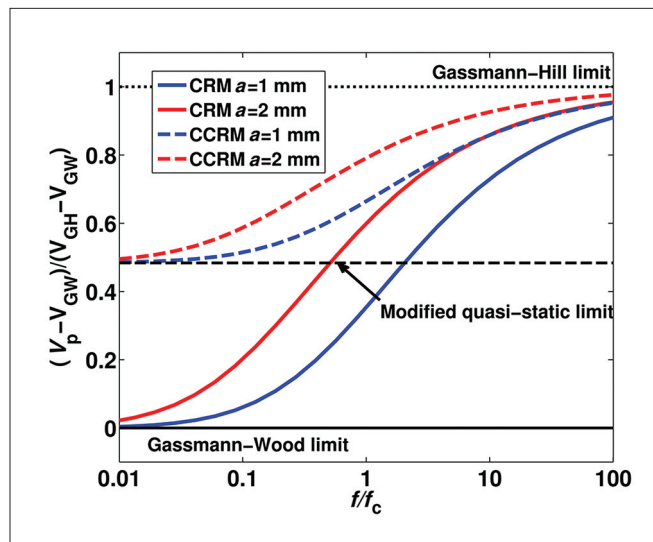


Figure 8. Dispersion relations for the CRM model (solid line) and its capillarity-extended version, CCRM (dashed line), for two correlation lengths a . The quasi-static limit increases in presence of capillarity and renormalizes the dispersion relation. V_{GW} and V_{GH} are the Gassmann-Wood and Gassmann-Hill velocities, respectively. The critical frequency (f_c) is 180 Hz for this numerical example.

in Figure 2 in a consistent way. The capillarity-extended CRM model predicts higher velocities and lower attenuation than the CRM model with statistical information from the CT images (black circles in Figure 2), thereby offering a meaningful modeling choice.

There is always a certain ambiguity when relating wave attenuation to the presence of fluid patches. That is because in real rock formations, it is likely that micro- and macroscopic heterogeneities other than fluid patches will interfere with the wave-induced pressure diffusion across fluid patches. For example, capillary forces can prevent fluid mixing so that in a fractured rock, the equant pores and fractures are saturated with different fluids. Then attenuation and dispersion are controlled by a combination of the background-fracture and fluid-fluid compressibility contrasts. For certain combinations, this can lead to complete annihilation of WIFF (Kong et al., 2013).

Another intriguing aspect comes into play when spatial-permeability variations are modeled. Then the diffusion length changes not simply with the square root of frequency (Caspari et al., 2013), and hence attenuation and dispersion also change (Rubino et al., 2013).

Conclusions

Attenuation- and velocity-saturation relations at different scales have been analyzed and interpreted in terms of the wave-induced pressure-diffusion mechanism. It appears that some inferences about the fluid-patch distribution can be made from those relations. Millimeter-sized fluid patches affect attenuation in the ultrasonic and sonic frequency bands. Centimeter-sized fluid patches can affect seismic attenuation if the fluid-compressibility contrast is high, such as

Downloaded 06/06/14 to 130.223.67.26. Redistribution subject to SEG license or copyright; see Terms of Use at http://library.seg.org/

in water-gas or brine-CO₂ systems. Laboratory experiments show that injection-rate changes during core flooding affect ultrasonic waveforms. That can be an indication that capillarity alters the fluid-patch distribution and thus affects ultrasonic wave attenuation. Further research is needed to understand whether those findings extend to the seismic frequency band. **TLE**

References

- Ajo-Franklin, J. B., J. Peterson, J. Doetsch, and T. M. Daley, 2013, High-resolution characterization of a CO₂ plume using crosswell seismic tomography: Cranfield, MS, USA: International Journal of Greenhouse Gas Control, **18**, 497–509.
- Alemu, B. L., E. Aker, M. Soldal, Ø. Johnsen, and P. Aagaard, 2013, Effect of sub-core scale heterogeneities on acoustic and electrical properties of a reservoir rock: A CO₂ flooding experiment of brine saturated sandstone in a computed tomography scanner: Geophysical Prospecting, **61**, no. 1, 235–250, <http://dx.doi.org/10.1111/j.1365-2478.2012.01061.x>.
- Biot, M. A., 1962, Mechanics of deformation and acoustic propagation in porous media: Journal of Applied Physics, **33**, no. 4, 1482–1498, <http://dx.doi.org/10.1063/1.1728759>.
- Caspari, E., T. M. Müller, and B. Gurevich, 2011, Time-lapse sonic logs reveal patchy CO₂ saturation in-situ: Geophysical Research Letters, **38**, no. 13, paper L13301, <http://dx.doi.org/10.1029/2011GL046959>.
- Caspari, E., B. Gurevich, and T. M. Müller, 2013, Frequency-dependent effective hydraulic conductivity of strongly heterogeneous media: Physical Review E: Statistical, Nonlinear, and Soft Matter Physics, **88**, no. 4, paper 042119.
- Kong, L., B. Gurevich, T. M. Müller, Y. Wang, and H. Yang, 2013, Effect of fracture fill on seismic attenuation and dispersion in fractured porous rocks: Geophysical Journal International, **195**, no. 3, 1679–1688, <http://dx.doi.org/10.1093/gji/ggt354>.
- Konishi, C., H. Azuma, D. Nobuoka, Z. Xue, and J. Watanabe, 2009, CO₂ saturation estimation from P-wave velocity changes by considering patchy saturation: Presented at the SEG Summer Research Workshop.
- Lebedev, M., J. Toms-Stewart, B. Clennell, M. Pervukhina, V. Shulakova, L. Paterson, T. M. Müller, B. Gurevich, and F. Wenzlau, 2009, Direct laboratory observation of patchy saturation and its effects on ultrasonic velocities: The Leading Edge, **28**, no. 1, 24–27, <http://dx.doi.org/10.1190/1.3064142>.
- Lei, X., and Z. Xue, 2009, Ultrasonic velocity and attenuation during CO₂ injection into water-saturated porous sandstone: Measurements using difference seismic tomography: Physics of the Earth and Planetary Interiors, **176**, nos. 3–4, 224–234.
- Lopes, S., and M. Lebedev, 2012, Research note: Laboratory study of the influence of changing the injection rate on the geometry of the fluid front and on P-wave ultrasonic velocities in sandstone: Geophysical Prospecting, **60**, no. 3, 572–580, <http://dx.doi.org/10.1111/j.1365-2478.2011.01009.x>.
- Lopes, S., M. Lebedev, T. M. Müller, M. B. Clennell, and B. Gurevich, 2014, Forced imbibition into a limestone: Measuring P-wave velocity and water saturation dependence on injection rate: Geophysical Prospecting, published online, <http://dx.doi.org/10.1111/1365-2478.12111>.
- Mavko, C., and T. Mukerji, 1998, Bounds on low-frequency seismic velocities in partially saturated rocks: Geophysics, **63**, no. 3, 918–924, <http://dx.doi.org/10.1190/1.1444402>.
- Müller, T. M., and B. Gurevich, 2004, One-dimensional random patchy saturation model for velocity and attenuation in porous rocks: Geophysics, **69**, no. 5, 1166–1172, <http://dx.doi.org/10.1190/1.1801934>.
- Müller, T. M., B. Gurevich, and M. Lebedev, 2010, Seismic wave attenuation and dispersion resulting from wave-induced flow in porous rocks — A review: Geophysics, **75**, no. 5, 75A147–75A164, <http://dx.doi.org/10.1190/1.3463417>.
- Rubino, J. G., L. B. Monachesi, T. M. Müller, L. Guarracino, and K. Holliger, 2013, Seismic wave attenuation and dispersion due to wave-induced fluid flow in rocks with strong permeability fluctuations: Journal of the Acoustical Society of America, **134**, 4742–4751.
- Rubino, J. G., C. L. Ravazzoli, and J. E. Santos, 2009, Equivalent viscoelastic solids for heterogeneous fluid-saturated porous rocks: Geophysics, **74**, no. 1, N1–N13, <http://dx.doi.org/10.1190/1.3008544>.
- Rubino, J. G., D. R. Velis, and M. D. Sacchi, 2011, Numerical analysis of wave-induced fluid flow effects on seismic data: Application to monitoring of CO₂ storage at the Sleipner field: Journal of Geophysical Research: Solid Earth, **116**, no. B3, paper B03306, <http://dx.doi.org/10.1029/2010JB007997>.
- Tserkovnyak, Y., and D. L. Johnson, 2003, Capillary forces in the acoustics of patchy-saturated porous media: Journal of the Acoustical Society of America, **114**, no. 5, 2596–2606, <http://dx.doi.org/10.1121/1.1621009>.
- Toms, J., T. M. Müller, and B. Gurevich, 2007, Seismic attenuation in porous rocks with random patchy saturation: Geophysical Prospecting, **55**, no. 5, 671–678, <http://dx.doi.org/10.1111/j.1365-2478.2007.00646.x>.
- Vasco, D. W., T. M. Daley, and A. Bakulin, 2014, Utilizing the onset of time-lapse changes: A robust basis for reservoir monitoring and characterization: Geophysical Journal International, **197**, no. 1, 542–556, <http://dx.doi.org/10.1093/gji/ggt526>.
- Villaudy, F., M. H. Grochau, P. M. Benac, N. Lucet, and C. E. B. S. Abreu, 2013, 4D simultaneous pre-stack inversion in an offshore carbonate reservoir: 13th International Congress of the Brazilian Geophysical Society, Extended Abstracts, 1–5.
- Xue, Z., D. Tanase, and J. Watanabe, 2006, Estimation of CO₂ saturation from time-lapse CO₂ well logging in an onshore aquifer, Nagaoka, Japan: Exploration Geophysics, **37**, no. 1, 19–29, <http://dx.doi.org/10.1071/EG06019>.
- Yu, G., N. Shah, M. Robinson, N. H. Nghi, A. A. Nurhono and G. S. Thu, 2012, Resolution improvement and stratigraphic interpretation for the thin turbiditic sands in offshore Sabah, Malaysia — A pilot study: 82nd Annual International Meeting, SEG, Expanded Abstracts, <http://dx.doi.org/10.1190/segam2012-0089.1>.

Acknowledgments: We wish to acknowledge the funding provided by the Australian government through the CRC Program to support CO2CRC research, the Australian Research Council Discovery-Project—DP1096232, Australia-China Natural Gas Technology Fund (contract number CTR-DJ-04194-1), CSIRO, the Curtin Reservoir Geophysics Consortium (CRGC), and the CIPRS scholarship.

Corresponding author: tobias.mueller@csiro.au